Available online at www.sciencedirect.com
ScienceDirect
Journal of Nuclear Materials 363–365 (2007) 1441–1445
journal of nuclear materials
www.elsevier.com/locate/jnucmat

Study of highly ionized Xe spectra with 3s–3p and 3p–3d transitions in JT-60U reversed shear plasmas

H. Kubo [a,*], A. Sasaki [b], K. Moribayashi [b], S. Higashijima [a], H. Takenaga [a], K. Shimizu [a], T. Nakano [a], A. Whiteford [c], T. Sugie [a]

[a] Fusion Research and Development Directorate, Japan Atomic Energy Agency, Mukoyama, Naka-shi 311-0193, Japan
[b] Quantum Beam Science Directorate, Japan Atomic Energy Agency, Kizu-cho, Souraku-gun 619-0215, Japan
[c] Department of Physics, University of Strathclyde, Glasgow G4 ONG, UK

Abstract

In JT-60U, Xe gas has been injected into reversed shear plasmas with internal transport barriers. During these discharges, spectra from highly ionized Xe atoms have been observed in a wavelength range of 4–16 nm. The observed spectra have been analyzed by calculating theoretical spectra for Xe XXXVII–XLV 3s–3p and 3p–3d transitions with relativistic atomic structure codes, a collisional radiative model, and an impurity transport code. Several lines for Xe XLI and XLII have been newly identified. Soft X-ray emission profiles have also been analyzed, and the results showed that the Xe ions accumulated inside the internal transport barrier.

PACS: 32.30.Jc; 32.30.−r; 52.55.Fa; 52.25.Vy

Keywords: Spectroscopy; Impurity; JT-60U; Impurity transport

1. Introduction

In next-step fusion reactors such as ITER, tungsten is a candidate material for the plasma facing components [1]. However, high-Z elements such as tungsten radiate more efficiently than low-Z elements and their accumulation is a concern for improved confinement plasmas [2]. On the other hand, radiation loss power enhancement is useful for mitigating the severe problem of concentrated power loading of the divertor plates, and controlled impurity gas injection is an effective technique for the radiation loss power enhancement [2,3]. In some tokamaks, Xe has been injected to study high-Z impurity behavior or to enhance radiation loss power [4,5]. For such studies, analysis of vacuum ultra-violet spectra from highly ionized Xe atoms is essential. However, little investigation has been performed on these spectra [6]. Actually, no lines have been identified for Xe XXX–XL 3s–3p and 3p–3d transitions.

In JT-60U, Xe has been injected into reversed shear plasmas with internal transport barriers (ITB) to study high-Z impurity transport. Spectra of highly ionized Xe emission for the 3s–3p and

* Corresponding author. Fax: +81 29 270 7419.
E-mail address: kubo.hirotaka@jaea.go.jp (H. Kubo).

0022-3115/$ - see front matter © 2007 Elsevier B.V. All rights reserved.
doi:10.1016/j.jnucmat.2007.01.232

3p–3d transitions have been observed and analyzed using relativistic atomic structure codes, a collisional radiative model, and an impurity transport code. Soft X-ray emission profiles have also been analyzed to investigate the Xe ions accumulated inside the ITB.

2. Experiment

Fig. 1 shows the plasma configuration and the diagnostics for the present study. Vacuum ultraviolet spectra were observed using a flat-field grazing incidence spectrometer with a holographic grating [7]. The spectrometer covered a wavelength range of 0.5–40 nm with a 1024 channel detector using micro channel plates. A VYNS window (10 mg/cm^2, 90% chloride, 10% vinyl acetate) [8] was set in the spectrometer to reduce stray light. The inverse linear dispersion was 0.044 nm/channel at 7 nm, and the wavelength resolution was ~0.075 nm (~1.7 channels). The wavelength was calibrated using C VI 3.3736 nm, B V 4.8588 nm, the second order line of C VI 3.3736 nm, and Fe XXIII 13.2906 nm. As a result, wavelengths of isolated spectral lines in a wavelength range of 4–16 nm could be determined with uncertainties of ~0.0044 nm (~0.1 channels) by fitting the spectral line shapes. The line-integrated electron densities were measured with two FIR interferometers, the electron temperature and density profiles were measured with a Thomson scattering system, and the soft X-ray emission (the energy range was 2.7–20 keV) profiles were measured with a PIN detector array.

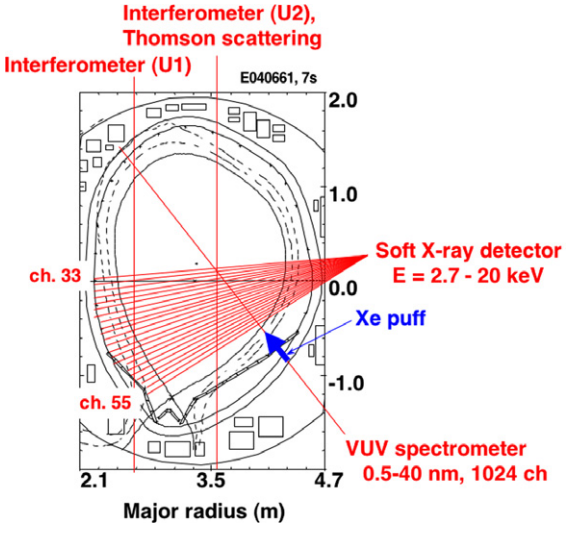

Fig. 1. The plasma configuration and the diagnostics for the present study. The position of the Xe gas puff is also shown.

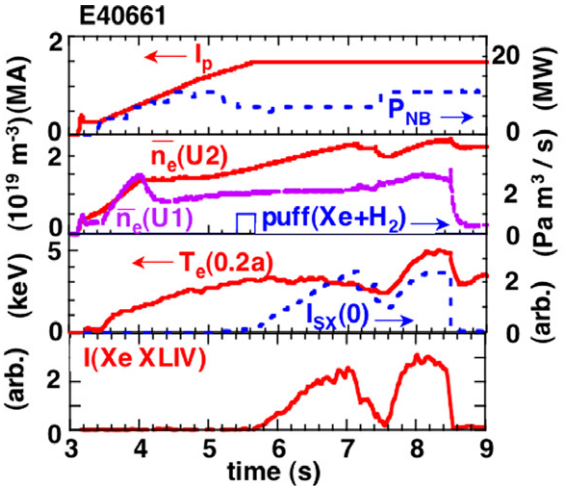

Fig. 2. Waveforms of a reversed shear plasma with Xe injection. I_p: plasma current, P_{NB}: NBI power, n_e: line-averaged electron densities measured with U1 and U2 chords (see Fig. 1), puff (Xe + H_2): puffing rate of Xe gas mixed with H_2 gas (the Xe volume fraction was 1/9.), T_e (0.2 a): electron temperature at $r = 0.2$ a, I_{SX}: intensity of the soft X-ray emission measured with the viewing chord passing the plasma center, I (Xe XLIV): intensity of Xe XLIV 3s $^2S_{1/2}$–3p $^2P_{3/2}$line. Here, a denotes the plasma minor radius.

Fig. 2 shows waveforms of a reversed shear plasma with Xe injection. While the plasma current was ramping up, beginning at ~5.0 s, the ITB developed, with the electron density in the core plasma (U2) increasing at a faster rate than that in the edge region (U1). The Xe gas (the Xe gas was mixed with H_2 gas to control such the small Xe injection rate with the gas valve) was injected at 5.4 s. The soft X- ray emission and the intensity of the Xe XLIV 3s $^2S_{1/2}$–3p $^2P_{3/2}$ line increased after 5.6 s. Collapses occurred at 7.1 and 7.4 s, and the soft X-ray emission and the Xe XLIV intensity decreased rapidly with the collapses and recovered after the collapses. The electron temperatures at the plasma center were 3.0 and 4.7 keV at 6.9 and 8.2 s, respectively.

3. Results and discussion

The radial profiles of the electron temperature and density at 6.9 s are shown in Fig. 3(a). An ITB was clearly observed in the profiles, and the electron temperature and density were almost constant inside of the ITB. Profiles of Xe^{z+} ion densities were calculated with a one-dimensional impurity

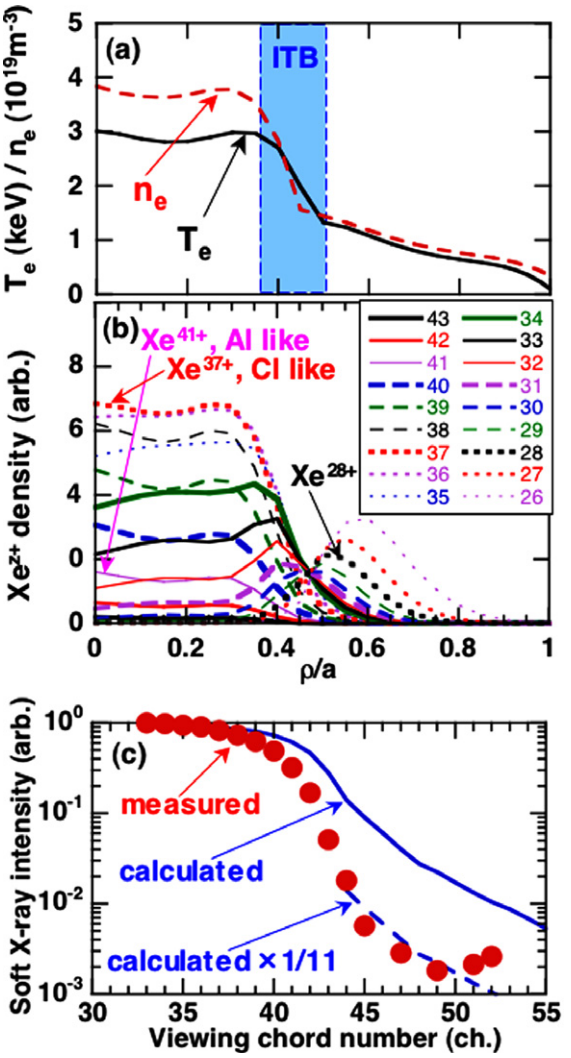

Fig. 3. Radial profiles of (a) the electron temperature and density, (b) the calculated Xe^{z+} ion densities, and (c) the measured and calculated soft X-ray intensity at 6.9 s. In the calculation, the total Xe ion density profile was assumed to be similar to the electron density profile. The soft X-ray intensity was normalized at 33 channel (see Fig. 1), and the broken curve indicates the calculated intensity multiplied by 1/11 for the edge region.

transport code. The radial Xe^{z+} ion flux $\Gamma_z(r)$ can be usually modeled as

$$\Gamma_z(r) = -D_z(r)\frac{\partial n_z(r)}{\partial r} + v_z(r)n_z(r), \quad (1)$$

where $n_z(r)$ is the Xe^{z+} ion density, $D_z(r)$ is the diffusion coefficient, and $v_z(r)$ is the inward velocity [9]. We took for the diffusion coefficients and inward velocities

$$D_z(r) = D = \text{constant}, \quad (2)$$

$$v_z(r) = c_v D\frac{\partial(\log n_e(r))}{\partial r}, \quad (3)$$

where c_v is a constant peaking factor. Then, the total Xe ion density profile, $\Sigma n_z(r)$, is given by

$$\sum n_z(r) \propto n_e(r)^{c_v}. \quad (4)$$

Here, we assumed that $D = 1\ \text{m}^2/\text{s}$ and $c_v = 1$, giving the total Xe ion density profile similar to the electron density profile. In the calculation, we used ionization and recombination rate coefficients from PPPL ADPAK [9,10]. The calculated Xe ion density profiles are shown in Fig. 3(b). The figure shows that Xe^{37+} (Cl-like) ion was dominant in the core plasma. The ion fractions inside the ITB were almost constant and close to the coronal equilibrium. As a result, it was expected that we could calculate spectral lines from the highly ionized Xe atoms inside the ITB using corona ionization equilibrium and a collisional radiative model with the electron temperature and density at the plasma center.

Soft X-ray emission profiles were calculated using soft X-ray emission rate coefficients considering the spectral detection coefficient of the detector [2,11]. The soft X-ray emission profile was analyzed by comparing it with the calculated one in Fig. 3(c). When the soft X-ray intensity profiles were normalized at the plasma center, the measured intensity was about one eleventh of the calculated intensity at the plasma edge. This indicates that the measured intensity profile was more peaked than the calculated profile. Hence, the total Xe ion density profile was not similar to the electron density profile and the Xe ions accumulated inside the ITB. Considering previous investigation on C, Ne and Ar ion transport [2], this result shows that accumulation is large for high-Z impurities. Although this tendency is qualitatively in agreement with the neoclassical transport theory, the quantitative accumulation is much smaller than the theoretical prediction [2].

Fig. 4(a) shows the spectra observed at 5.4 s (just before the Xe injection), 6.9 s and 8.2 s. Many spectral lines from highly ionized Xe atoms appeared after the Xe injection. The spectra were analyzed by comparing spectra calculated for Xe XXXVII–XLV (Ar-like – Ne-like) using relativistic atomic structure codes, a collisional radiative model, and coronal ionization equilibrium model. For the collisional radiative model, HULLAC [12] was used.

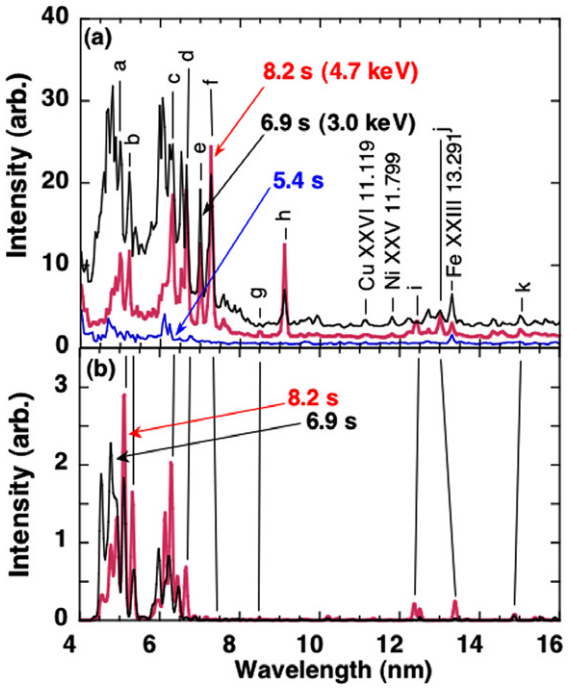

Fig. 4. (a) Observed and (b) calculated spectra. The observed spectra were corrected for the transmittance of the VYNS window. Since the VYNS window has absorption edges at 4.2, 4.3, and 5.9 nm, the spectra can be distorted there. For the calculated spectra, line broadening due to the wavelength resolution of the spectrometer was considered. The calculation was performed using the measured electron temperatures and densities inside the ITB ($T_e = 3.0$ keV and $n_e = 4.0 \times 10^{19}$ m^{-3} at 6.9 s, and $T_e = 4.7$ keV and $n_e = 4.0 \times 10^{19}$ m^{-3} at 8.2 s). The labels of the Xe lines refer to those in Table 1.

The coronal ionization equilibrium was calculated using ADPACK, and the results showed that Xe^{37+} (Cl-like) and Xe^{41+} (Al-like) ions were dominant at 3.0 and 4.7 keV, respectively. Although HULLAC can also calculate the wavelengths, the wavelengths calculated with a multiconfiguration relativistic Dirac–Fock program of Desclaux [13] were used for the calculation, since the wavelengths calculated with the Desclaux code are considered to be more accurate than those calculated with HULLAC. The calculated spectra are shown in Fig. 4(b). The calculation shows that Xe XXXVII–XLV 3s–3p and 3p–3d lines appeared in the wavelength range. Emission in a wavelength range of 4.4–5.5 nm was dominantly ascribed to 3p–3d transitions of Xe XXXVII–XLIV. The wavelengths of the 3p–3d lines tend to increase with the charge number of the ions in the wavelength range. This tendency can explain difference in the spectra between 6.9 and 8.2 s; as the electron temperature

Table 1
Observed and calculated spectral lines of Xe ions

Label	Ion	Lower level			Upper level			Present observation			Previous observation		Calculation	
		Configuration	Term	J	Configuration	Term	J	Wavelength	Intensity	Comments	Wavelength		Wavelength	A
a	Xe XLI	$3s^2\,3p^2$	^{3}p	0	$3s^2\,3p\,3d$	^{3}D	1	4.993(0.022)	7	Blend(P-like)	–		5.1149	3.52E+11
b	Xe XLII	$3s^2\,3p$	^{2}P	1/2	$3s^2\,3d$	^{2}D	3/2	5.212(0.013)	8	Blend(short)	–		5.322	2.30E+11
f	Xe XLII	$3s^2\,3p$	^{2}P	3/2	$3s^2\,3d$	^{2}D	5/2	7.274(0.006)	19	–	–		7.378	1.05E+11
k	Xe XLII	$3s^2\,3p$	^{2}P	1/2	$3s^2\,3p$	^{2}P	3/2	15.031(0.015)	0.9	–	–		14.861	2.71E+06
c	Xe XLIII	$3s^2$	^{1}S	0	3s 3p	^{1}P	1	6.300(0.014)	9	Blend(short)	6.288(0.003)[a]		6.2904	3.15E+11
j	Xe XLIII	$3s^2$	^{1}S	0	3s 3p	^{3}P	1	13.006(0.008)	2.3	–	12.993(0.003)[b]		13.386	6.79E+09
d	Xe XLIV	3s	^{2}S	1/2	3p	^{2}P	3/2	6.661(0.005)	16	–	6.658(0.003)[c]		6.654	1.61E+11
g	Xe XLIV	3p	^{2}P	3/2	3d	^{2}D	5/2	8.496(0.006)	0.6	–	8.48(0.05)[d]		8.492	6.63E+10
i	Xe XLIV	3s	^{2}S	1/2	3p	^{2}P	1/2	12.403(0.007)	1.9	–	12.392(0.003)[c]		12.369	2.40E+10
–	Xe XLIV	3p	^{2}P	1/2	3d	^{2}D	3/2	–	–	Edge	5.91(0.1)[d]		5.825	1.69E+11
e	Xe	–	–	–	–	–	–	7.000(0.005)	10	Unclassified	–		–	–
h	Xe	–	–	–	–	–	–	9.110(0.006)	11	Unclassified	–		–	–

The units of wavelength, intensity, and A (transition probability) are nm, arbitrary, and s^{-1}, respectively. Uncertainties of the observed wavelengths are shown in the parentheses. The intensity was measured at 8.2 s. The b and c lines had blends in the short wavelength sides, and the a line was blended with a line from the Xe XL ion.
The references of the previous observation are [a] Ref. [14], [b] Ref. [15], [c] Ref. [16], [d] Ref. [17].
The calculation results were obtained using the Desclaux code [13]. The emission from Xe XLII $3s^2\ 3p\ ^2P_{1/2}$–$3s^2\ 3p\ ^2P_{3/2}$ is due to magnetic dipole radiation.

increased, emission around 5 nm became stronger than that around 4.5 nm. The observed and calculated Xe spectral lines are summarized in Table 1. In addition to previously observed Mg-like and Na-like ion lines, several lines from Al-like and Si-like ions were newly identified. For the wavelengths, the present observation almost agreed with the previous observation within the uncertainties. In the present observation, the wavelength of Xe XLIV $3p\ ^2P_{1/2}$–$3d\ ^2D_{3/2}$ was not identified due an absorption edge of the VYNS filter. We classified the f line as Xe XLII $3s^2\ 3p\ ^2P_{3/2}$–$3s^2\ 3d\ ^2D_{5/2}$, although the calculated intensity was low. For light species such as Fe, it is often observed that the $3s^2\ 3p\ ^2P_{3/2}$–$3s^2\ 3d\ ^2D_{5/2}$ line is strong comparably to the $3s^2\ 3p\ ^2P_{1/2}$ – $3s^2\ 3d\ ^2D_{3/2}$ line, since the $3s_2\ 3p\ ^2P_{3/2}$ level is appreciably populated and the population of the $3s^2\ 3d\ ^2D_{5/2}$ is produced by collisional excitation from the $3s_2\ 3p\ ^2P_{3/2}$ level. On the other hand, for heavy species such as Xe, the population of the $3s_2\ 3p\ ^2P_{3/2}$ level becomes small in low-density plasmas such as tokamak plasmas due to the large excitation energy and the high radiative decay rate. However, even for Ag XXXV, it has been observed that the line is rather strong in tokamak plasmas [18]. Further investigation is needed to understand the line emission. Two strong lines (e and h lines) have not been classified, and further investigation for these lines is also needed.

4. Summary

In JT-60U, Xe was injected into reversed shear plasmas with internal transport barriers, and spectra of highly ionized Xe atoms with 3s–3p and 3p–3d transitions were observed in a wavelength range of 4–16 nm and analyzed using relativistic atomic structure codes, a collisional radiative model, and an impurity transport code. The observed spectra were compared with calculated spectra for Xe XXXVII–XLV 3s–3p and 3p–3d transitions. Several lines have been newly identified. However, the calculation could not explain some strong line emission. To establish spectroscopic diagnostics of high-Z impurity behavior in fusion plasmas, further investigation on spectra from highly ionized atoms of high-Z species is necessary. The atomic data and collisional radiative model should be improved. Soft X-ray emission profiles have been also analyzed, and the results indicated that the Xe ions accumulated inside the ITB. Control of high-Z impurity behavior in improved confinement plasmas with ITBs is an important issue.

Acknowledgements

The authors are grateful to Professor H. Summers of University of Strathclyde for support of this work and Dr M. Nagami of Japan Atomic Energy Agency for useful discussion. They express their thanks to Drs E.B. Saloman and J. Reader of National Institute of Standards and Technology for providing Xe spectral data.

References

[1] G. Federici et al., Nucl. Fus. 41 (2001) 1967.
[2] H. Kubo et al., J. Nucl. Mater. 313–316 (2003) 1197.
[3] H. Kubo et al., Nucl. Fus. 41 (2001) 227.
[4] K.W. Hill et al., Phys. Plasmas 6 (1999) 877.
[5] R. Dux et al., Nucl. Fus. 39 (1999) 1509.
[6] E.B. Saloman, J. Phys. Chem. Ref. Data 33 (2004) 765.
[7] H. Kubo et al., Rev. Sci. Instrum. 59 (1988) 1515.
[8] J.E. Manson, Solar Phys. 27 (1972) 107.
[9] R.A. Hulse, Nucl. Technol–Fusion 3 (1983) 259.
[10] D. Post et al., Atom Data Nucl. Data 20 (1977) 397.
[11] H.P. Summers, Atomic Data and Analysis Structure Users Manual, Rep. JET-IR 06, JET Joint Undertaking, Abingdon (1994) (H.P. Summers, 2004, The ADAS User Manual Version 2.6 <http://adas.phys.strath.ac.uk>.).
[12] A. Bar-Shalom, et al., in: D.R. Schultz, et al., (Ed.), Atomic Processes in Plasmas: 13th APS Topical Conf., American Institute of Physics, 2002, p. 92.
[13] J.P. Desclaux, Comput. Phys. Comm. 9 (1975) 31.
[14] J.O. Ekberg et al., Phys. Scr. 43 (1991) 19.
[15] J.F. Seely et al., J. Opt. Soc. Am. B 5 (1988) 602.
[16] J.F. Seely et al., Phys. Rev. A 38 (1990) 5246.
[17] E. Träbert et al., Z. Phys. 32 (1995) 295.
[18] E. Hinnov et al., J. Opt. Soc. Am. B 3 (1986) 1288.